Available online at www.sciencedirect.com
SCIENCE DIRECT®
Acta Materialia 53 (2005) 79–86
Acta MATERIALIA
www.actamat-journals.com

# Curvature driven grain boundary migration in aluminum: molecular dynamics simulations

H. Zhang [a,b,*], M. Upmanyu [c], D.J. Srolovitz [a,b]

[a] Department of Mechanical and Aerospace Engineering, Princeton University, Princeton, NJ 08540, USA
[b] Princeton Institute for the Science and Technology of Materials, Princeton University, Princeton, NJ 08540, USA
[c] Materials Science Program, Division of Engineering, Colorado School of Mines, Golden, CO 80401, USA

Received 20 April 2004; received in revised form 9 September 2004; accepted 11 September 2004
Available online 13 October 2004

**Abstract**

Molecular dynamics simulations have been used to study steady-state, capillarity-driven grain boundary migration in three dimensions for a series of ⟨1 1 1⟩-tilt boundaries in aluminum. The reduced boundary mobility and boundary enthalpy were determined as a function of misorientation and temperature. For the misorientations examined, the reduced mobility is a maximum and the activation energy for migration is a minimum at the Σ7 misorientation. The reduced mobility is an Arrhenius function of temperature. Excellent agreement between the present three-dimensional simulation results, those obtained earlier in two dimensions and experiment is obtained for a wide variety of features, with the notable exception of the magnitude of the grain boundary mobility. The mobilities from the simulations are much higher than from experiment; the activation energies for migration are much lower. The present results are intrinsic, while the experimental measurements may be limited by extrinsic factors such as impurity drag.


*Keywords:* Grain boundary migration; Molecular dynamics; Simulation; Aluminum

## 1. Introduction

The thermodynamics and kinetics of grain boundaries is central to microstructural evolution in a variety of materials systems. Grain boundary migration controls the evolution kinetics during materials processing, thus determining microstructural parameters such as grain size and texture. Since grain size affects strength and other materials properties, it is one of the key microstructural parameters considered in the optimization of such processes as annealing, hot rolling, extrusion, and forging. The evolution of grain size is controlled largely by grain boundary migration processes. Therefore, understanding grain boundary migration is central to the development of microstructure evolution modeling.

Grain boundary studies performed on polycrystalline samples can be used to obtain the temporal evolution of the average grain size and, hence, the average grain boundary mobility. However, since this averaging is biased towards grain boundaries that occur more frequently than random, it is difficult to interpret the meaning of such average properties. Reasonable alternatives include measuring the properties of individual grain boundaries in bicrystals or deconvoluting the properties of individual boundaries from the evolution of polycrystals with spatially local crystallographic measurements. Bicrystal experiments have been based upon a variety of different grain boundary geometries (planar, wedge-shaped, half and quarter loop) and have been used to

* Corresponding author. Tel.: +1 609 258 2775; fax: +1 609 258 6878.
*E-mail address:* hzhang@princeton.edu (H. Zhang).

1359-6454/$30.00 © 2004 Acta Materialia Inc. Published by Elsevier Ltd. All rights reserved.
doi:10.1016/j.actamat.2004.09.004

extract the temperature, driving force and crystallographic dependence of boundary migration rates [1–19]. The experimental findings can be summarized as follows:

(a) The migration rate is proportional to the driving force, provided that drag effects are minimized (e.g., from grain boundary grooving) [13].
(b) The temperature dependence of the migration rate can be described as Arrhenius [9,15,17].
(c) The migration rate and the activation energy of migration are non-monotonic functions of grain boundary misorientation $\theta$, with extrema at or near many high symmetry, low $\Sigma$CSL [20] grain boundaries [7,8,12,18,21,22].
(d) There is no correlation between grain boundary diffusion and grain boundary mobility (although, the minima in grain boundary mobility was shown to correlate with the maxima in grain boundary diffusion in some cases) [4,8,15,23,24].
(e) Grain boundary migration is very sensitive to the presence of impurities in most cases [8,12,19,22,25].

Of all the bicrystal geometries employed in experimental studies, the half- and quarter-loop geometries are unique in permitting measurements to be made in true steady-state using capillarity driving forces [16]. Recently, the same bicrystal geometry has been adopted to study grain boundary migration in two-dimensional, atomistic computer simulations [26,27]. This simulation approach has some advantages over experiments, including the complete elimination of impurities and precise control over such parameters as the orientations of the two crystals, temperature, stress, etc. Schönfelder et al. [28] and Zhang et al. [29] have also performed three-dimensional molecular dynamics (MD) simulation of boundary migration using elastic strain to drive boundary migration. All of the simulations showed that the rate of boundary migration was proportional to the driving force and the boundary mobility was an Arrhenius function of temperature. Detailed examination of the activation energies for migration as a function of misorientations showed excellent correspondence between simulation and experiment. However, the activation energies obtained from atomistic simulations were invariably significantly smaller than those found in experiments (even in high purity materials) [27–30].

While the extant two-dimensional simulations, performed over a wide range of bicrystallography, were in good agreement with many facts of the experimental data, the appropriateness of direct comparisons between such simulations and three-dimensional experiments remains uncertain. On the other hand, the existing three-dimensional simulations considered only a very limited set of boundaries and were often based on overly simplistic descriptions of atomic interactions [28]. The present study addresses these issues through three-dimensional simulations with more realistic interatomic potentials. In particular, we perform three-dimensional, half-loop molecular dynamics simulations of the steady-state migration of a series of high angle, $\langle 1\,1\,1\rangle$ tilt grain boundaries in aluminum using EAM (embedded atom method) interatomic potentials [31]. In the next section, the theoretical basis for the analysis of grain boundary migration is introduced and simulation details are provided. The next section presents the main simulation results (reduced grain boundary mobilities as a function of driving force, temperature and bicrystallography). These results are compared with earlier two-dimensional Lennard-Jones simulation results obtained using the same simulation method [26,27] and the existing experimental data [18,23,32]. Finally, we discuss the significance of the results and summarize our main conclusions.

## 2. Simulation method

Based upon absolute-reaction rate theory ideas, Turnbull [33,34] showed that the grain boundary velocity $v$ may be written as mobility $M$ times driving force $F$:

$$v = MF, \quad M = M_0 \exp\left[\frac{-Q_{gb}}{k_B T}\right], \tag{1}$$

where $Q_{gb}$ is the activation energy (enthalpy) for grain boundary migration, $k_B T$ is the thermal energy and $M_0$ is a constant. For curvature-driven boundary migration, the driving force is associated with the decrease in net grain boundary energy [35]. Hence, Eq. (1) becomes

$$v = M(\gamma_{gb} + \gamma''_{gb})\kappa, \tag{2}$$

where $\kappa$ is the grain boundary curvature $\gamma_{gb}$ and $\gamma''_{gb}$ are the grain boundary free energy and its second derivative with respect to boundary inclination, respectively, and $\gamma_{gb} + \gamma''_{gb}$ is known as the grain boundary stiffness. We use Eq. (2) to analyze the simulation results, as described below.

Fig. 1 shows the three-dimensional, U-shaped half-loop bicrystal simulation cell used to extract steady-state intrinsic grain boundary properties. The two grains are initially perfect face centered cubic crystal, misoriented with respect to each other by a rotation about a common $\langle 1\,1\,1\rangle$-axis (the $Z$-axis in Fig. 1). Periodic boundary conditions are applied along the $X$- and $Z$-directions. The atoms in the four atomic layers closest to the $Y = 0$ plane are fixed to prevent grain rotation and maintain the half-loop width, $w$. The opposite face of the simulation cell is left free to relax the elastic stresses that develop due to the removal of the excess volume associated with the decrease in grain boundary area.

Assuming self-similar migration and the validity of Eq. (2), the velocity of the top of the half-loop can be shown to be

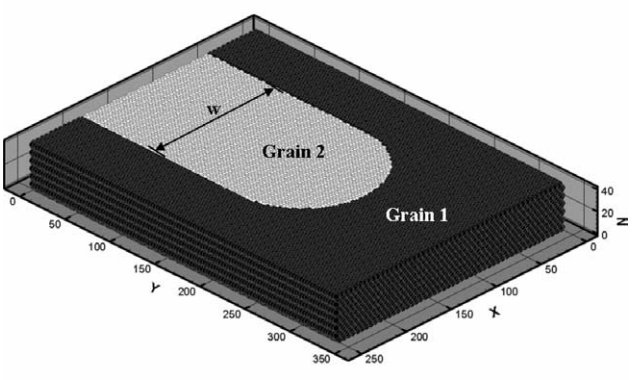


Fig. 1. The initial half-loop, bicrystal geometry employed in the molecular dynamics simulations.

$$\upsilon = M(\gamma_{gb} + \gamma''_{gb})\left(\frac{\pi}{w}\right) = M^*\left(\frac{\pi}{w}\right), \tag{3}$$

where $M^*$ is the reduced grain boundary mobility. The rate of change of the volume of the half-loop grain is then

$$\dot{V} = \upsilon w z = M^* \frac{\pi}{w} w z = M^* \pi z, \tag{4}$$

where $z$ is the thickness of the bicrystal in the $z$-direction. Eq. (4) suggests that the reduced grain boundary mobility is proportional to the rate of change of the volume of Grain 2. The reduction in the volume of Grain 2 is driven by the decrease in total grain boundary area $A_{gb}$. The rate of decrease in free energy $E$ of the simulation cell is given by

$$\dot{E} = \bar{\gamma}_{gb} \frac{\partial A_{gb}}{\partial t} = 2z\bar{\gamma}_{gb} \frac{\partial}{\partial t}\left(\frac{V}{wz}\right) = 2\bar{\gamma}_{gb}\dot{V}/w \tag{5a}$$

or

$$\bar{\gamma}_{gb} = \left(\frac{w}{2}\right)\frac{\dot{E}}{\dot{V}}, \tag{5b}$$

where $\bar{\gamma}_{gb}$ is the average of the grain boundary free energies (per unit area) of the two parallel flat segments of the half-loop parallel to the $Y$-axis. (Note, we have implicitly assumed that the half-loop is infinitely long and that the migration is steady-state.) The total free energy of the system cannot be easily extracted from the present, non-equilibrium MD simulations. However the internal energy of the system $U$ is readily available from the simulations, and enables us to extract the grain boundary enthalpy, $\bar{\gamma}^H_{gb}$,

$$\bar{\gamma}^H_{gb} = \left(\frac{w}{2}\right)\frac{\dot{U}}{\dot{V}}. \tag{6}$$

Note that since the migrating grain boundary is curved in the present half-loop simulations, the grain boundary mobility is implicitly averaged over boundary inclination.

The present MD simulations were performed in the canonical NVT ensemble. Each simulation included approximately 200,000 atoms. The simulation cell contained 18 {1 1 1} atomic planes and was at least 20, 34 and 4.2 nm along the $X$-, $Y$- and $Z$-directions, respectively. The interactions between the atoms were described using the Voter–Chen EAM potential for Al [31]. This is one of a large number of EAM-type of potentials for Al and has been widely applied. This potential yields the correct elastic constants, vacancy formation energy, cohesive energy, lattice parameter, interatomic spacing (properties to which it was fitted) and reasonable interface properties for Al, for example, the calculated average surface energy for (1 1 1) is 824 mJ/m$^2$ compared to experimental value is 980 ± 150 mJ/m$^2$ [31,36]. However, it yields a melting point which is significantly lower than in experiment (i.e., $T_m$ was estimated to be 610 K [37]) and a vacancy migration barrier (0.30 eV) which is about half of the experimental value (0.65 eV). The simulations were performed on a parallel computer using a message-passing interface (MPI) in which the simulation space was divided between different processors using neighbor lists [38] and linked cells [39], as described in [40]. The equations of motion were integrated using a velocity-Verlet algorithm [38,41,42]. The temperature was fixed during the simulation using the well-known Nose–Hoover thermostat [43,44], as described in [45].

In order to measure the rate of change of volume of the half-loop grain (Grain 2), we must first identify to which grain each atom belongs. This is accomplished by examining the local orientation of the neighborhood of each atom with respect to an external frame of reference. We employ the following symmetry parameter for atom $i$:

$$f_i = \frac{1}{n}\sum_{i=j}^{n}\left[(3 - 4\sin^2\theta_{ij})^2 \sin^2\theta_{ij}\right], \tag{7}$$

where the sum is over the $n$ atoms within a distance of $1.2r_{nn}$ of atom $i$, where $r_{nn}$ is the spacing between nearest neighbors in the crystal at the temperature of interest. If we project the vector connecting atom $i$ with atom $j$ on to the $X$–$Y$ plane, $\theta_{ij}$ is the angle between this vector and the unit vector in the $X$-direction. A unique value of $f$ exists for each crystal orientation (modulo the rotational symmetry). Therefore, if the symmetry factor for atom $i$, $f_i$, is closer to that of Grain 1 than to that of Grain 2, it is assigned to Grain 1. The values of the volume of Grain 2, $V(t)$, and the energy of the system, $U(t)$, used in the determination of the migration rates and the grain boundary enthalpy are each averaged over at least three independent time periods during the course of a single simulation run.

The initial bicrystal was constructed by rotating Grain 2 with respect to the [1 1 1] axis of Grain 1, and

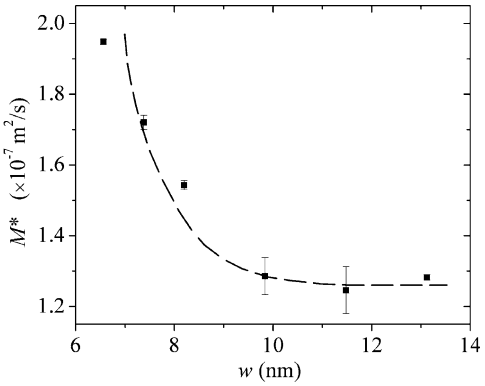


Fig. 2. The reduced mobility as a function of half loop width.

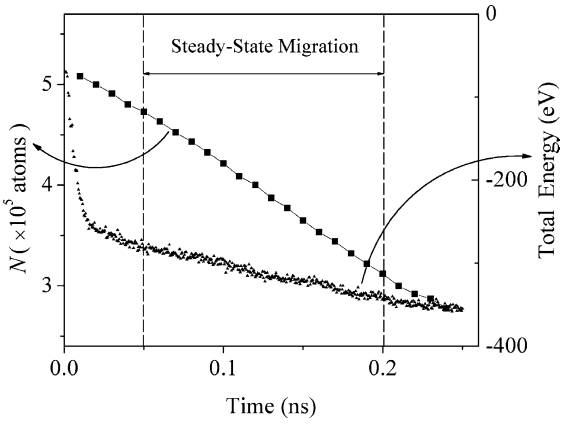


Fig. 3. The number of atoms in the half-loop grain $N$ vs. simulation time at 427 K in a simulation with a misoriention of 38.2° and a half-loop width of $w = 12$ nm. The plot also shows the variation of the total energy of the simulation cell with time (the zero of energy was arbitrarily fixed for convenience).

removing all of the atoms from Grain 2 outside the half-loop shape and removing all of the atoms from Grain 1 within the half-loop. If any two atoms were closer together than 90% of the equilibrium inter-atomic separation, one of the pair of atoms was removed. In order to allow the half-loop to migrate over sufficiently long distances such that steady-state kinetic is achieved, the computational cell is at least $3w$ in the $Y$-direction and $2w$ in the $X$-direction where $w$ is the half loop width. These dimensions were chosen to insure that the free and frozen surfaces did not interfere with the boundary migration process. Fig. 2 shows a plot of reduced mobility of a $\theta = 36°$ $\langle 1\,1\,1\rangle$ tilt grain boundary as function of the half-loop width 6.5 nm $< w <$ 13.2 nm, at $T = 366$ K. For $w \geqslant 10$ nm, the reduced mobility is independent of half-loop width, as expected. Therefore, all simulations reported below were performed with half-loop widths in excess of 10 nm. Our simulations also show that the boundary mobility is independent of the cell thickness for $z > 3.5$ nm (15 $\langle 1\,1\,1\rangle$ planes). Hence, all simulations reported below were performed using $z = 4.2$ nm (18 $\langle 1\,1\,1\rangle$ planes).

## 3. Simulation results

Fig. 3 shows the temporal evolution of the number of atoms in the half-loop $N(t)$ for a $\theta = 38.2°$ $\langle 1\,1\,1\rangle$ tilt grain boundary, for simulation performed with $w = 12$ nm at 427 K. Following an initial transient associated with the relaxation of the as-constructed boundary structure and one at the end of the simulation where the top of half-loop is too close to the bottom of the simulation cell, the number of atoms in the half-loop (or grain volume) decreases linearly with time. This is indicative of steady state, curvature driven grain boundary motion. This trend in migration behavior is reproduced in all simulations. As mentioned in the previous section, the slope associated with the linear decrease yields the reduced mobility of the grain boundary, $M^* = M(\gamma_{gb} + \gamma'')$. The reported values of the reduced mobility, below, are averages over three slope measurements made at different times in the half-loop retraction in which the rate of change of the number of atoms is constant.

The effect of misorientation on the reduced mobility for $\langle 1\,1\,1\rangle$ boundaries is shown in Fig. 4 for high-angle misorientations in the range $26° < \theta < 42°$ for $T = 305$, 366 and 427 K. The maximum reduced mobility occurs at the misorientations corresponding to the high symmetry $\Sigma 7$ boundary, $\theta = 38.2°$, where $\Sigma$ is the coincident site lattice density (see e.g. [20]). Within the accuracy of the present data, no such maximum occurs at the misorientations corresponding to the next highest symmetry, i.e., $\Sigma 13$ $\theta = 27.8°$. On the other hand, the reduced mobility exhibits a minimum at misorientations close to $\theta = 30°$. As the temperature increases, the ratio of the maximum ($\Sigma 7$ $\theta = 38.2°$) to the minimum ($\theta = 30°$) reduced mobility decreases from $\sim$8 at $T = 305$ K to $\sim$3 at $T = 427$ K.

The misorientation dependence of the reduced mobility of the $\langle 1\,1\,1\rangle$ tilt grain boundaries in Al has also been

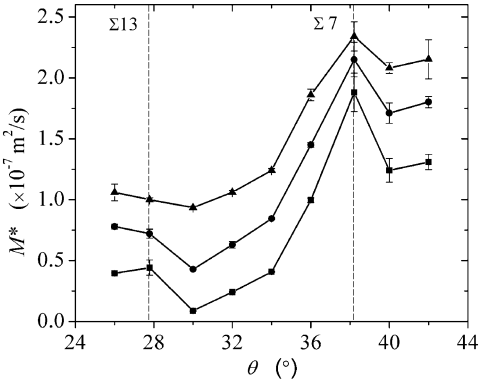


Fig. 4. Reduced mobility as a function of misorientation at three different temperatures. Squares, circles and triangles represent simulation results at temperatures 305, 366 and 427 K, respectively.

experimentally extracted using a similar capillarity-driven boundary migration geometry in similar misorientation and temperature ranges [32]. Although it is difficult to extract regular trends from the experimental data over the entire misorientations range, a few clear conclusions can be drawn: (i) raising the temperature increases the magnitude of the reduced mobility, (ii) increasing the temperatures decreases the ratio of the maximum to minimum reduced mobilities (in the $25° < \theta < 42°$ range), and (iii) the $\Sigma 7$ 38.2° misorientations corresponds to a local maximum in the reduced boundary mobility. These are all in agreement with the simulation observations of Fig. 4. On the other hand, the minimum in the reduced mobility observed at ~30° in the simulation does not appear in the experimental data nor does an apparent minimum at ~35° observed in the experiment appear in the simulation data. It is difficult to determine the significance of this comparison, however, given that the experimental reduced mobilities are about three orders of magnitude smaller than those found from the simulations. This has been attributed to the influence of impurities on grain boundary migration in the experimental system [27].

The variation of the reduced boundary mobility with temperature is shown in Fig. 5 for four different misorientations in Arrhenius form (i.e., $\ln M^*$ vs. $1/T$). Although the data are somewhat sparse, this figure shows that each data set lies on a straight line. This implies that reduced mobility can be described as an Arrhenius function of temperature, as suggested in Eq. (1). This suggests that boundary migration is thermally activated. Fitting the data to the form $M_0^* \exp(-Q_{gb}/k_B T)$ allows us to extract the activation energy (slope) and pre-exponential factor (intercept) in the Arrhenius expression. Examination of the inset to this figure for the $\Sigma 7$ $\theta = 38.2°$ misorientation and those closest to it (i.e., 36° and 40°), show that the all three lines extrapolate through approximately the same point. This corresponds to a temperature of 497 K or 0.81 $T_m$, where $T_m$ is the melting point for this interatomic potential [37]. Examination of the experimental data [46] shows that the reduced mobilities for several misorientations near $\Sigma 7$ are nearly equal at 770 K or 0.82 $T_m$, where $T_m$ is the experimental melting point of Al. Clearly, the simulations and experiment are in excellent agreement.

The misorientation dependence of the activation energies and pre-exponential factors ($M_0^*$) for boundary migration are shown in Fig. 6(a) and (b) (based on linear fits to the data in Fig. 5 and similar plots for the other misorientations). The variations of the activation energies and the logarithms of the pre-exponential factor with misorientation are very similar. Both show local minima at the high symmetry $\Sigma 7 - \theta = 38.2°$ and $\Sigma 13 - \theta = 27.8°$ misorientations. The nature of this correlation may be seen more clearly in Fig. 7, where we plot $\ln M_0^*$ vs. $Q$ for different misorientations. While all of the data fall very close to a single straight line, the correlation between $\ln M_0^*$ and $Q$ is particularly good for misorientations in the vicinity of $\Sigma 7 - \theta = 38.2°$ (see the inset to Fig. 7). This is consistent with the observation that the $\ln M^*$ vs. $1/T$ data, for misorientations near $\Sigma 7$, extrapolate through a single point (Fig. 5). It

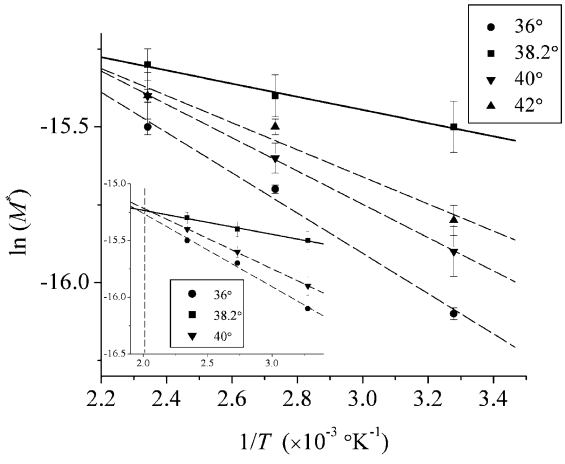


Fig. 5. Logarithm of the reduced mobility (in units of $10^{-7}$ $m^2/s$) vs. inverse temperature for four different misorientations near 38.2°, the $\Sigma 7$ misorientation. The inset shows the extrapolation of the data for the $\Sigma 7$ and two closest misorientations to higher temperatures.

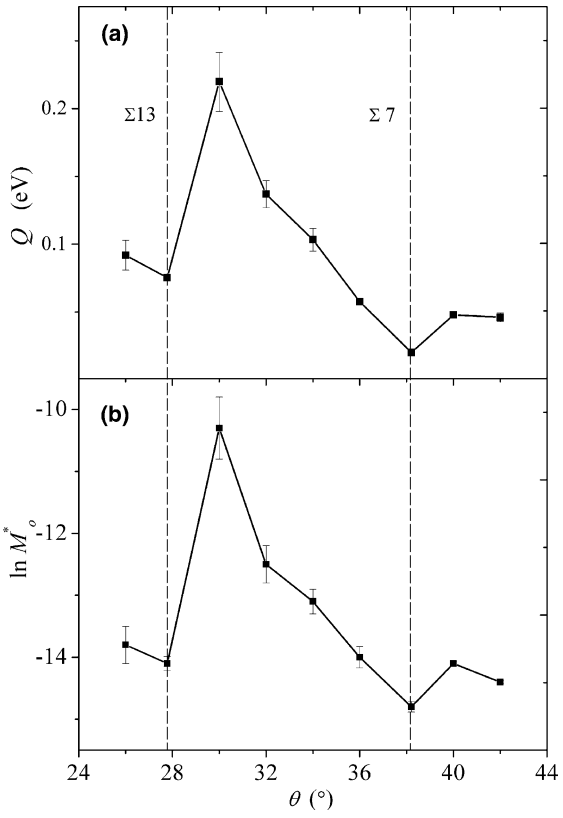


Fig. 6. The (a) activation energy and (b) logarithm of the pre-exponential factor (in units of $10^{-7}$ $m^2/s$) for boundary migration as a function of misorientation.

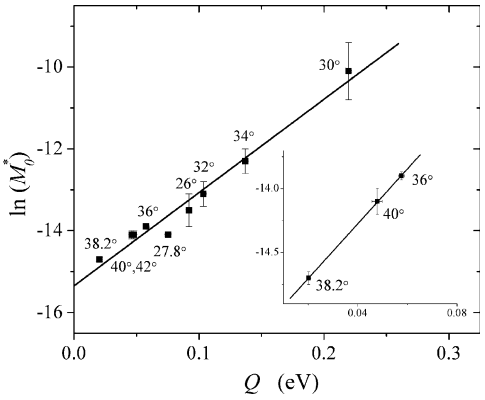


Fig. 7. Logarithm of the pre-exponential factor (in units of $10^{-7}$ m$^2$/s) as a function of activation energy. The inset only shows the data for $\Sigma 7$ and its two closest misorientations.

is also consistent with experimental observations on Al in the vicinity of $\Sigma 7$ [18]. The strong correlation between the activation energies and logarithms of the pre-exponential factor are indicative of the fact that the variation of the reduced mobilities with misorientation is much weaker than would be expected based upon the activation energy itself.

Since the reduced mobility is the product of the grain boundary mobility and the interfacial stiffness (see Eqs. (2) and (3)), extraction of the grain boundary mobility itself from the simulation data requires knowledge of the grain boundary free energy and its variation with boundary inclination. Unfortunately, we have not extracted this quantity. However, the simulations can be used to extract the grain boundary enthalpy $\bar{\gamma}^{\mathrm{H}}_{\mathrm{gb}}$ as a function of misorientation, as described above (see Eq. (6)). This data are shown in Fig. 8 for $T = 427$ K. While small minima are observed for the high symmetric grain boundary misorientations, the dominant feature in Fig. 8 is the presence of a strong maximum at $\theta = 30°$. This misorientation also corresponds to a minimum in the reduced mobility (Fig. 4) and maxima in both $\ln M_0^*$ and $Q$.

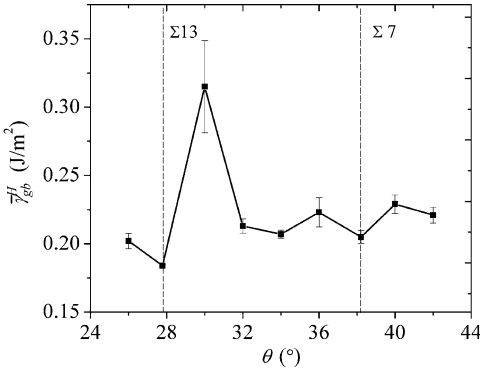


Fig. 8. The average grain boundary enthalpy as a function of grain boundary misorientation at 427 K.

## 4. Discussion and conclusion

In this paper, we examined steady-state, capillarity-driven grain boundary migration in three dimensions on an atomic scale using the molecular dynamics simulation method and an EAM-type potential fit to the properties of Al. In particular, we focused on the reduced grain boundary mobility as a function of bicrystallography (grain misorientation) and temperature. The reduced mobility as a function of misorientation (in the range 26–42°) showed a maximum at the misorientation corresponding to the high symmetry $\Sigma 7$ misorientation ($\langle 1\,1\,1\rangle$ tilt boundary separating grains that are misoriented by 38.2°). At fixed misorientation, the reduced mobility can be described in terms of an Arrhenius function of temperature. The activation energy is a local minimum at the $\Sigma 7$ misorientation. The logarithm of the pre-factor in the Arrhenius relation for the reduced mobility, $\ln M_0^*$, was shown to be approximately proportional to the activation energy for grain boundary migration over the entire misorientation range considered. This correlation was especially strong for the $\Sigma 7$ misorientation and misorientations close to it. Arrhenius plots of $\ln M^*$ vs. $1/T$ for these misorientations all cross at (near) a single temperature – the so-called compensation temperature [47]. Similar correlations and crossings have been observed experimentally [18]. Although the melting temperature predicted using the current EAM potential is much lower than found in experiment, the compensation temperature for those misorientations near $\Sigma 7$ was found to be $\sim 0.81\ T_{\mathrm{m}}$ in the simulations and $\sim 0.82\ T_{\mathrm{m}}$ in experiments on the same material [46]. Although we were unable to determine the free energy of the migrating boundaries, we determined the grain boundary enthalpy to be in the range of 0.18–0.32 J/m$^2$. A strong maximum in the boundary enthalpy appeared at a misorientation of $\theta \approx 30°$. Experimentally, the average high angle grain boundary energy was determined to be 0.32 J/m$^2$ in Al [48].

The reduced mobility in the misorientation range examined here (26–42°) is not a simple function of misorientation. It exhibited maxima at 38.2° ($\Sigma 7$) at all temperatures and at 27.8° ($\Sigma 13$) at the lowest temperature ($0.5\ T_{\mathrm{m}}$), minima at $\sim 30°$ and $\sim 40°$ at all temperatures, and was smooth in between these extrema. The maximum at the $\Sigma 7$ misorientation appeared to be a cusp, while the other extrema were not as sharp. (Note, the reduced mobilities quoted are averages over all possible inclinations.) Experimental measurements of the reduced mobility for the same boundaries show the same general trends, although it is somewhat less systematic [32]. All of the experimental data and the earlier molecular dynamics simulations performed in two dimensions using a Lennard-Jones potential [27] also show a strong maximum at the $\Sigma 7$ misorientation. Although the two-

dimensional simulations showed a clear maximum at the $\Sigma 13$ misorientation grain boundary, the evidence for such a maximum in the experimental and three-dimensional simulation date is not as strong.

The origin of the maxima in the reduced mobility at high symmetry misorientations remains uncertain. It may be attributable to the existence of a more ordered grain boundary structure at these misorientations. This could translate into higher mobilities through a decrease in the number of atoms involved in the fundamental event that leads to migration or simply to a reduced barrier for the local reorientation. However, we cannot rule out the possibility that it is associated with the non-mobility contribution to the reduced mobility, i.e., the boundary stiffness. While the grain boundary enthalpy is a local minimum at the high symmetry misorientations, the behavior of the stiffness (which includes a term that is the second derivative of the boundary free energy with respect to boundary inclination) may be a maximum at these special misorientations.

The magnitude of the reduced mobility for the boundaries examined here was found to range from $10^{-11}$ to $10^{-9}$ $m^2/s$ at $0.72T_m$ in experiment [32]. In our three-dimensional simulations, the reduced mobility varies from $10^{-8}$ to $10^{-7}$ $m^2/s$ at $0.7T_m$. The discrepancy between the experimental and simulation data is 2–3 orders of magnitude. This difference may be attributable to the presence of a (very) small concentration of impurities in the experimental system which is not present in the simulations. Although the impurity concentrations may be very small, on average, the concentration at the grain boundary may be significant – giving rise to impurity drag. The reduced mobilities measured in the simulations should be viewed as intrinsic, while the reduced mobility in the experiments may be limited by extrinsic factors.

Another possible reason why the simulations yield much higher mobilities than observed experimentally may be associated with the interatomic potential employed. This concern may be heightened by the observation that the potential yields values for melting point and vacancy formation energy that are too low. However, the present simulations yield much higher mobilities than seen in experiment at the same homologous temperature ($T/T_m$). We can estimate the effect of the low melting point of the simulated Al by scaling the simulated activation energy by the ratio of the experimental and simulation melting points. Using this scaling, the corrected average activation energy from the simulation would be 0.14 eV rather than the unscaled activation energy of 0.09 eV. Clearly, the discrepancy in the melting points cannot account for the difference between the simulation and experimental ($\sim$2 eV) activation energies for grain boundary migration. Recent simulations [30] of the stress-driven migration of planar boundaries in Al using both a new EAM potential (fit to a wide range of crystal, crystal defect, and liquid data) [30] and the Ercolessi–Adams EAM potential [49] (the melting point and vacancy migration energy for both potentials is close to the experimental values) yielded very high grain boundary mobilities, as compared with experiment. This suggests that the observation of much higher mobilities in simulations than in experiment is robust; i.e., this observation is relatively insensitive to the choice of interatomic potential.

In order to compare the activation energies for boundary migration determined from the present three-dimensional simulations, earlier two-dimensional simulations and experiments, it is important to appropriately normalize the data. This is necessary because the two-dimensional results were performed using an unrealistic interatomic potential and a different crystal lattice (triangular lattice rather than face centered cubic). One approach to normalizing the data from different potentials and crystal structures is to define an energy scale as the cohesive energy divided by the number of nearest neighbor bonds, $z$, (and another factor of two to avoid double counting); i.e., $\varepsilon = 2E_{coh}/z$. The average normalized activation energy for capillarity driven boundary migration (activation energy divided by $\varepsilon$) from experiment [18] is $\sim$3, from the two-dimensional simulations [27] is 0.4 and the present three-dimensional simulations is 0.2. This shows that the observation of very low activation energies for grain boundary migration seen in simulations is also robust with respect to the dimensionality of the simulations [27–30]. Therefore, the most probable explanation of the observation that grain boundary mobilities seen in simulations are very much larger than those seen in experiment is associated with impurity drag effects.

## Acknowledgement

The authors gratefully acknowledge useful discussions with Dr. S.G. Srivilliputhur, Dr. A.F. Voter and Dr. S.P. Chen and the support of the US Department of Energy, Grant No. DE-FG02-99ER45797 and Computational Materials Science Network.

## References

[1] Beck PA. Trans Am Inst Min Eng 1940;152:103.
[2] Anderson WA, Mehl RF. Trans Am Inst Min Metall Eng 1945;161:140.
[3] Dunn CG, Daniels FW, Bolton MJ. Trans Am Inst Min Metall Eng 1949;185:708.
[4] Burke JE, Turnbull D. Recrystallization and grain growth. Progress in metal physics. Oxford: Pergamon Press; 1949.
[5] Fullman RL. Boundary migration during grain growth. Metal interfaces. ASM Press; 1952.
[6] Mullins WW. Acta Metall Mater 1956;4:421.

[7] Aust KT, Harrison EH, Maddin R. J I Met 1956;85:15.
[8] Aust KT, Rutter JW. Trans Am Inst Min Metall Eng 1959;215:119.
[9] Aust KT, Rutter JW. Trans Am Inst Min Metall Eng 1959;215:820.
[10] Rutter JW, Aust KT. Trans Am Inst Min Metall Eng 1960;218:682.
[11] Rutter JW, Aust KT. Acta Metall Mater 1965;13:181.
[12] Demianczuk DW, Aust KT. Acta Metall Mater 1975;23:1149.
[13] Rath BB, Hu H. T Metall Soc Aime 1969;245:1243.
[14] Sun RC, Bauer CL. Acta Metall Mater 1970;18:635.
[15] Sun RC, Bauer CL. Acta Metall Mater 1970;18:639.
[16] Aristov VY, Fradkov VE, Shvindlerman LS. Sov Phys Solid State 1980;22:1817.
[17] Gottstein G, Czubayko U, Molodov DA, Shvindlerman LS, Wunderlich W. Mater Sci Forum 1996;204:99.
[18] Molodov DA, Czubayko U, Gottstein G, Shvindlerman LS. Scr Metall Mater 1995;32:529.
[19] Furtkamp M, Lejcek P, Tsurekawa S. Interface Sci 1998;6:59.
[20] Sutton AP, Balluffi RW. Interfaces in crystalline materials. Oxford: Clarendon Press; 1995.
[21] Beck PA, Sperry PR, Hu H. J Appl Phys 1950;21:420.
[22] Gottstein G, Shvindlerman LS. Scr Metall Mater 1992;27:1515.
[23] Gottstein G, Molodov DA, Shvindlerman LS. Interface Sci 1998;6:7.
[24] Molodov DA, Swiderski J, Gottstein G, Lojkowski W, Shvindlerman LS. Acta Metall Mater 1994;42:3397.
[25] Cole DG, Feltham P, Gillam E. Proc Phys Soc London B 1954;67:131.
[26] Upmanyu M, Smith RW, Srolovitz DJ. Interface Sci 1998;6:41.
[27] Upmanyu M, Srolovitz DJ, Shvindlerman LS, Gottstein G. Acta Mater 1999;47:3901.
[28] Schönfelder B, Wolf D, Phillpot SR, Furtkamp M. Interface Sci 1997;5:245.
[29] Zhang H, Mendelev MI, Srolovitz DJ. Acta Mater 2004;52:2569.
[30] Mendelev MI, Srolovitz DJ, Han S, Ackland GJ, Morris JR. Phys Rev B 2004 [submitted].
[31] Voter AF, Chen SP. Mater Res Soc Symp Proc 1987;82:175.
[32] Aristov VY, Mirochnik VL, Shvindlerman LS. Sov Phys Solid State 1976;18:137.
[33] Turnbull D. Trans Am Inst Min Metall Eng 1951;191:661.
[34] Smoluchowski R. Phys Rev 1951;83:69.
[35] Herring C. Surface tension as a motivation for sintering. The physics of powder metallurgy. New York: McGraw-Hill; 1951.
[36] Chen SP, Voter AF, Srolovitz DJ. Phys Rev Lett 1986;57:1308.
[37] Srinivasan SG. Private communication.
[38] Verlet L. Phys Rev 1967;159:98.
[39] Allen MP, Tildesley DJ. Computer simulation of liquids Oxford: Clarendon Press; 1987.
[40] Srinivasan SG, Ashok I, Jonsson H, Kalonji G, Zahorjan J. Comput Phys Commun 1997;102:28.
[41] Verlet L. Phys Rev 1968;165:201.
[42] Hansen JP, Verlet L. Phys Rev 1969;184:151.
[43] Nose S. J Chem Phys 1984;81:511.
[44] Hoover WG. Phys Rev A 1985;31:1695.
[45] Hoover WG, Holian BL. Phys Lett A 1996;211:253.
[46] Molodov DA, Czubayko U, Gottstein G, Shvindlerman LS. Acta Mater 1998;46:553.
[47] Gottstein G, Shvindlerman LS. Grain boundary migration in metals: thermodynamics, kinetics, applications. Boca Raton (FL): CRC Press; 1999.
[48] Humphreys FJ, Hatherly M. Recrystallization and related annealing phenomena. Oxford: Pergamon Press; 2002.
[49] Ercolessi F, Adams JB. Europhys Lett 1994;26:583.